Copula density-driven Metrics for Sensitivity Analysis: Theory and application to Flow and Transport in porous media.

Aronne Dell'Oca, Alberto Guadagnini, and Monica Riva

Department of Civil and Environmental Engineering, Politecnico di Milano, 20133, Milan, Italy;

Corresponding author: Aronne Dell'Oca (aronne.delloca@polimi.it)

Accepted Manuscript

Dell'Oca, A., A. Guadagnini, and M. Riva (2020), Copula density-driven Metrics for Sensitivity Analysis: Theory and application to Flow and Transport in porous media, *Adv. Water Resour.*, 145, 103714, 1-11. https://doi.org/10.1016/j.advwatres.2020.103714.

Abstract

We introduce original sensitivity analysis metrics with the aim of assisting diagnosis of the functioning of a given model. We do so by characterizing model-induced dependencies between a target model output and selected model input(s) through the associated bivariate copula density. The latter fully characterizes the dependencies between two random variables at any order (i.e., without being limited to linear dependence), independent of the marginal behavior of the two variables. As a metric to assess sensitivity, we rely on the absolute distance between the copula density associated with the target model output and a model input and its counterpart associated with two independent variables. We then provide two sensitivity indices which allow characterizing (*i*) the global (with respect to the input) value of the sensitivity and (*ii*) the degree of variability (across the range of the input values) of the sensitivity for each value that the prescribed model output can possibly undertake, as driven by the governing model. In this sense, our approach to sensitivity is *global* with respect to model input(s) and *local* with respect to model output, thus enabling one to discriminate the relevance of an input across the entire range of values of the modeling goal of interest. We exemplify the use of our approach and illustrate the type of information it can provide by focusing on an analytical test function and on two scenarios related to flow and transport in porous media.

Plain Language Summary

Modern models of environmental systems have reached a relatively high level of complexity. The latter aspect could hamper a clear understanding of the way a model functions, i.e., how it drives relationships and dependencies among inputs and outputs of interest. A rigorous Sensitivity Analysis can contribute to solve this issue. We propose here to characterize the nature of pairwise model input-output dependencies through their copula density. The latter enables one to identify the strength of (nonlinear) dependencies between two variables and is independent from the format of their marginal distributions. We also provide two sensitivity indices to characterize, for each value of the model output: (*a*) the average strength of the model-induced dependencies and (*b*) the variability of such dependences across the space of any model input parameter. Our methodology can be viewed as *global* with respect to the input and *local* with respect to the output, in the sense that it allows to naturally characterize sensitivity across the entire range of the target model outcomes.

1.Introduction

One of the main goals of a Global Sensitivity Analysis (GSA) is to provide enhanced understanding of the model considered to represent a target physical system (e.g., Gupta and Razavi, 2018 and references therein). Within the context of a GSA, the sensitivity of a modeling goal (or model output) to the (often uncertain) model input(s) is evaluated across the entire range(s) of variability of the latter, i.e., globally. This is in contrast to Local Sensitivity Analyses (LSA), where sensitivity is evaluated in the neighborhood of a set of model inputs, i.e., locally (e.g., Pianosi et al., 2016; Razavi and Gupta, 2015). As such, a GSA approach enables us to naturally account for model input uncertainties that are typically encountered in geophysical and hydrological models (e.g., Ceriotti et al., 2019; Di Fusco et al., 2018; Porta et al., 2018; Di Palma et al., 2017; Oladyshkin et al., 2012; Delfs et al., 2009; van Werkhoven et al., 2009; Tebes-Steven and Valocchi, 2000).

The variance-based Sobol' Indices (e.g., Sobol, 2001) represent one of the most widespread GSA metrics. The Principal Sobol' Index associated with a model input is defined as the average (hence its global nature) reduction in the variance of a model output stemming from knowledge of the input, normalized by the unconditional output variance. In this sense, the variance of the model output is at the core of the definition of sensitivity based on Sobol' indices. As such, the latter could provide at best an incomplete picture of a model behavior in the presence of skewed and/or heavy tailed probability density functions (*pdf*) of the output of interest, i.e., when the variance is an incomplete descriptor of the output uncertainty. Moment-independent GSAs (e.g., Pianosi and Wagner, 2015; Borgonovo, 2007) have been developed to cope with this issue. These approaches introduce a sensitivity metric which corresponds to a suitable distance between the unconditional *pdf* (or the cumulative distribution function, *CDF*) and its counterpart conditional to model input(s) values. The global nature of the sensitivity analysis is ensured by averaging this sensitivity metric across the support of the (random) model input(s). Along the same lines, an Information Theory-based GSA (Krzykacz-Hausmann, 2001) identifies sensitivity as the mutual information (i.e., a measure of the dependence among two variables; see e.g., Chang et al., 2016) between a model input and an output, normalized by the entropy of the latter. Mutual Information coincides with the difference between (*a*) the entropy of the unconditional model output *pdf* and (*b*) the averaged (with respect to the input) entropy of the model output *pdf* conditional to the input. The recently developed moment-based GSA (Dell'Oca et al., 2017) allows characterizing global sensitivity in terms of diverse features of the *pdf* of the output, as rendered by its statistical moments. Note that all of the methodologies illustrated above ground sensitivity on the comparison between conditional and unconditional features of the *pdf* (or *CDF*) of the modeling goal of interest.

Another aspect of sensitivity is tackled through the evaluation of a measure of the variations of the model output associated with corresponding changes in the model input(s). For example, approaches based on the Morris' Indices (Morris, 1991) or on the Distributed Evaluation of LSA (DELSA; Rakovec et al., 2014) essentially rest on the (local) concept of derivative to evaluate the strength of the variations imprinted to model outputs by input variations. The resulting metric is then subject to averaging across the input(s) space of variability, to render a global nature of the analysis. The VARS (Razavi and Gupta, 2016) approach introduces a measure of the variations by relying on the concept of variogram, as applied to the model response surface. The latter approach allows discerning the output-input(s) sensitivity over diverse scales of input(s) variability.

A third category of GSAs relies on the concept of correlation (e.g., Pearson Correlation Coefficient (CC), partial CC, Spearman Rank CC, or partial Rank CC; see e.g., Marino et al., 2009) between input and output. Along a similar line of approach, regression-based GSAs rescale the coefficient(s) of a regression expression between input(s) and model output to quantify the sensitivity of the latter with respect to the former (e.g., Pianosi et al., 2016 and reference therein). Xiao et al., (2018) introduce a correlation index relying on the concept of distance correlation (Székely et al., 2007) to assist sensitivity analyses in the case of multivariate model output. Da Veiga (2015) illustrates how diverse sensitivity indices (e.g., the principal Sobol' index, the moment-independent index of Borgonovo (2007), or the index proposed by Krzykacz-Hausmann (2001) and grounded on mutual information) can be obtained as special cases of a general dissimilarity measure between unconditional and conditional *pdf*s of a model output Lozzo and Marrel (2016) provide a study of diverse measures of dependence in the context of sensitivity analyses, focusing on the screening of model inputs.

Crick et al. (1987) highlight the distinction between *important* and *sensitive* model inputs, where the former are those whose uncertainty has the largest contributions to the output uncertainty, the latter being those having a significant influence on the output. Hamby (1994) remarks that an important input is always a sensitive one, while the opposite may not hold in case there is only little uncertainty about the input. In this context, GSA methodologies of the first category illustrated above could be viewed as more oriented towards quantification of importance of input(s), while methodologies of the other categories are interpreted as more oriented towards a characterization of the input influence, even as this type of distinction might not always be sharply delineated.

All of the GSA approaches illustrated above quantify the global sensitivity (or importance) of a model input to an output through summary indices/coefficients. In this sense, there is a unique value for a sensitivity index across the whole range of values the model output (y) can possible undertake and these GSA approaches do not enable one to answer questions such as "Is sensitivity stronger for low or high values of the output?", or "Are there regions (or values) in the space of variability of the output, as driven by the structure of the model employed, that are not sensitive to one or more model inputs?". Answer to these kinds of questions are intimately tied to a variety of studies (e.g., risk assessment and decision making under uncertainty) which are routinely conducted for hydrological systems. Here, we propose an original complement to the category of GSA approaches, aimed at characterizing sensitivity (following the definition of Crick et al., 1987) for each specific value that y can be possibly undertaken. We accomplish this by defining two sensitivity indices (for each value of y) grounded on the intensity/strength of the dependencies that the employed model induces between input and target output.

To characterize the input-output dependencies, we rely on elements of the theory underpinning bivariate copula. The latter has the key advantage of revealing the dependencies between two variables at any order (i.e., without being limited to a linear dependence) and regardless of the format of their marginal *CDF*s. We leverage on the bivariate copula density (e.g., Nelsen 2013; Bárdossy, 2006) between the target model output and each of the model inputs to quantify the dependencies induced by the model of choice. We define a suitable metric to measure sensitivity in this context and provide two distinct SA indices that allow characterizing (*i*) the global (with respect to the space of variability of model input) intensity of the sensitivity and (*ii*) the degree of variability of the output sensitivity across the range of values of the input, both aspects being evaluated for each value that the model output can assume.

While the approach we present can be transferred to diagnose models describing various hydrological and environmental scenarios, we exemplify its salient elements by (*i*) considering an analytical test function, which enables us to illustrate the type of information we can obtain under completely controlled conditions, and then (*ii*) focusing on two relatively simple scenarios which have been previously studied and are associated with the evaluation of the critical pumping rate that can be extracted from a well placed in a coastal aquifer (Pool and Carrera, 2011) and a laboratory-scale setting employed to analyze conservative transport within a heterogeneous porous medium (Esfandiar et al., 2015).

2. Methodology

Here we recall some basic concepts of bivariate copula (Section 2.1) and illustrate the main theoretical and operational elements of our GSA approach (Section 2.2).

2.1 Bivariate Copula

A function $C:[0,1]^2 \rightarrow [0,1]$ is defined as a bivariate copula when C is a joint *CDF* of a two-dimensional random vector (u_1, u_2) on the support $[0, 1]^2$ with uniform marginals (e.g., Nelsen, 2013)

$$C(u_1,u_2) = \Pr(U_1 \le u_1, U_2 \le u_2)\,, \tag{1}$$

where U_1 and U_2 are two random variables whose marginal *CDFs* are uniform.

Following Sklar (1973), a continuous bivariate joint *CDF*, $F(\psi_1, \psi_2)$, between two random variables ψ_1 and ψ_2 can be represented through a bivariate copula, i.e.,

$$F(\psi_1, \psi_2) = C(F_{\Psi_1}(\psi_1), F_{\Psi_2}(\psi_2)), \tag{2}$$

$F_{\Psi_1}(\psi_1)$ and $F_{\Psi_2}(\psi_2)$ being the marginal *CDFs* of ψ_1 and ψ_2, respectively.

The copula C in (2) is unique only if $F_{\Psi_1}(\psi_1)$ and $F_{\Psi_2}(\psi_2)$ are continuous, being otherwise uniquely determined on the support $Ran\, F_{\Psi_1} \times Ran\, F_{\Psi_2}$, *Ran* denoting range (e.g., Sklar, 1996). Considering the equivalence between u_i (i = 1, 2) in (1) and $F_{\Psi_i}(\psi_i)$ in (2), one can see that a given bivariate copula $C(u_1, u_2)$ can be associated with diverse formats for the marginal *CDFs*, i.e., $F_{\Psi_1}(\psi_1)$ and $F_{\Psi_2}(\psi_2)$. In other words, a bivariate copula encapsulates the dependences between two random variables regardless the format of their marginal distributions. Additionally, a bivariate copula can be used to describe dependencies between two random variables at any order, without being confined to first-order or linear relationships (as embedded, e.g., in the Pearson correlation coefficient; see e.g., Most et al., 2016). According to Bárdossy (2006), inspection of the bivariate copula density, i.e.,

$$c(F_{\Psi_1}(\psi_1), F_{\Psi_2}(\psi_2)) = \frac{\partial^2 C(F_{\Psi_1}(\psi_1), F_{\Psi_2}(\psi_2))}{\partial F_{\Psi_1}(\psi_1) \partial F_{\Psi_2}(\psi_2)}, \tag{3}$$

yields improved and straightforward understanding of the dependencies between $F_{\Psi_1}(\psi_1)$ and $F_{\Psi_2}(\psi_2)$ (and thus between ψ_1 and ψ_2). Regions of high/low value of the copula density are characterized by a strong/weak dependence between the corresponding values of the two random variables. Given its powerful and convenient properties to characterize a model-induced dependence between uncertain model inputs and a target output, we select the copula density as the basic descriptor upon which we ground our GSA.

2.2 Global Sensitivity Metrics based on copula density

In this study we structure our GSA according to the following four steps:

(*i*) we select the bivariate copula density, i.e., $c(F_{\Theta_n}(\theta_n), F_Y(y))$, between the *n*-th uncertain model input parameter, Θ_n, and the model output of interest, *Y*, as the descriptor underpinning SA;

(*ii*) we take the copula density associated with two statistically independent random variables, i.e., $c = 1$, as the reference value for the descriptor. Note that this choice renders a general, i.e., model independent, value for the reference descriptor;

(*iii*) we propose a simple metric to quantify sensitivity, i.e., $\left|1 - c(F_{\Theta_n}(\theta_n), F_Y(y))\right|$. Note that this metric has a local nature w.r.t. both the input and the output, i.e., it is defined for each $F_{\Theta_n}(\theta_n)$ and $F_Y(y)$;

(*iv*) we provide and evaluate two copula-based Global (w.r.t. the input) Sensitivity indices, as described in the following by (4) and (6).

The first copula-based Global Sensitivity index, I_{Θ_n}, is defined as

$$I_{\Theta_n} = \frac{1}{2} E_{F_{\Theta_n}} \left[\left| 1 - c\left(F_{\Theta_n}(\theta_n), F_Y(y) \right) \right| \right] \qquad \text{with} \qquad E_{F_{\Theta_n}}[\xi] = \int_{[0,1]} \xi dF_{\Theta_n}(\theta_n). \tag{4}$$

Index I_{Θ_n} is directly related to the expected value (w.r.t. $F_{\Theta_n}(\theta_n)$) of the absolute distance between the copula density of two independent random variables and the copula density of the random variables Θ_n and *Y*, $c(F_{\Theta_n}(\theta_n), F_Y(y))$. Note that $c(F_{\Theta_n}(\theta_n), F_Y(y))$ quantifies the dependencies between Θ_n and *Y*, as imprinted by the selected model. One can see that I_{Θ_n} is a function of $F_Y(y)$, i.e., I_{Θ_n} enables us to quantify the averaged (across all values of $F_{\Theta_n}(\theta_n)$) dependencies between *Y* and Θ_n when varying $F_Y(y)$. For example, if $I_{\Theta_n} = 0$ for some values of $F_Y(y)$, the associated values of *Y* are not sensitive to any of the values of Θ_n (i.e., the former are independent from the latter). Otherwise, if $I_{\Theta_n} = 1$ for some $F_Y(y)$, then the copula exhibits singular components for these $F_Y(y)$ (e.g., Nelsen, 2013; Chang et al., 2016; Durante et al., 2013), i.e., for these $F_Y(y)$, the specific value of the model output, *Y*, is dictated by that of Θ_n. Correspondences of the latter kind can be readily detected by (*a*) the direct analysis of the model at hand and/or (*b*) visual inspection of the scatter plot among the Grades of Θ_n, Grade(θ_n), and of *Y*, Grade(*y*) (see also Section 3.1). We recall that Grades are the population analogs of ranks (see also Section 2.1) and a scatterplot among Grades can be reconstructed also when the copula density displays singularities.

Note that index I_{Θ_n} does not provide information about the degree of variability of the sensitivity metric, i.e., $\left|1 - c(F_{\Theta_n}(\theta_n), F_Y(y))\right|$, across $F_{\Theta_n}(\theta_n)$ for diverse values of $F_Y(y)$. For example, it is possible that the same value I_{Θ_n} can be associated with two distinct values of $F_Y(y)$, one of which being characterized by a strong dependency that is concentrated within a narrow range of $F_{\Theta_n}(\theta_n)$ (i.e., given $F_Y(y)$, $c(F_{\Theta_n}(\theta_n), F_Y(y))$ displays high values only for a narrow range of $F_{\Theta_n}(\theta_n)$), the other one displaying a milder dependence that is otherwise more uniformly distributed across the entire range of $F_{\Theta_n}(\theta_n)$ (i.e., given $F_Y(y)$, $c(F_{\Theta_n}(\theta_n), F_Y(y))$ exhibits a mild strength/intensity over a broad range of $F_{\Theta_n}(\theta_n)$).

A straightforward quantification of the degree of variability in the sensitivity of $F_Y(y)$ across the range of values of $F_{\Theta_n}(\theta_n)$ can be obtained by considering a companion index, defined as the standard deviation (in the space of $F_{\Theta_n}(\theta_n)$) of $\left|1 - c(F_{\Theta_n}(\theta_n), F_Y(y))\right|$, i.e.,

$$\tilde{I}^*_{\Theta_n} = \sigma_{F_{\Theta_n}} \left[\left| 1 - c(F_{\Theta_n}(\theta_n), F_Y(y)) \right| \right] \qquad \text{with} \qquad \sigma_{F_{\Theta_n}}[\xi] = \sqrt{\int_{[0,1]} \left(\xi - E_{F_{\Theta_n}}[\xi] \right)^2 dF_{\Theta_n}(\theta_n)}. \tag{5}$$

As a limiting case, one can note that $\tilde{I}^*_{\Theta_n} = 0$ when $F_Y(y)$ is insensitive to all $F_{\Theta_n}(\theta_n)$ (i.e., $\left|1 - c(F_{\Theta_n}(\theta_n), F_Y(y))\right| = 0, \forall \ F_{\Theta_n}(\theta_n)$). Otherwise, $\tilde{I}^*_{\Theta_n} \to \infty$ for values $F_Y(y)$ for which the copula exhibits singular components. The latter aspect prompts us to introduce the following index

$$I^*_{\Theta_n} = 1 - e^{-\tilde{I}^*_{\Theta_n}} . \tag{6}$$

The latter ranges between zero (when $\tilde{I}^*_{\Theta_n} = 0$) and one (when $\tilde{I}^*_{\Theta_n} \to \infty$), thus allowing a straightforward comparison among values of the indices related to diverse (uncertain) model inputs.

Note that indices described by (4) and (6) provide a way to characterize sensitivity (*a*) in a local fashion (i.e., for each $F_Y(y)$ with respect to model output) and (*b*) globally (i.e., across all values of $F_{\Theta_n}(\theta_n)$) with respect to model input(s). Note that, even as the indices (4) and (6) are defined in terms of $F_Y(y)$, the information they provide can be readily mapped in terms of *y*. For completeness, it is worth noting that averaging index I_{Θ_n} w.r.t. $F_Y(y)$ yields the copula-based coefficient of correlation proposed by Chang et al. (2016).

We remark that the sensitivity metric introduced in the context of the density-based sensitivity analysis (see, e.g., Borgonovo, 2007; Borgonovo et al., 2016) is defined as $\left| p_{\Theta_n}(\theta_n) p_Y(y) - p_{\Theta_n,Y}(\theta_n, y) \right|$, where $p_{\Theta_n,Y}(\theta_n, y)$ is the bivariate *pdf* between the input Θ_n and the output *Y* and $p_{\Theta_n}(\theta_n) p_Y(y)$ is its counterpart under the assumption that Θ_n and *Y* are independent. Such a metric is then averaged (and multiplied by 1/2) with respect to both Θ_n and *Y*, resulting in the so-called δ_{Θ_n} index (see Appendix B). Thus, index δ_{Θ_n} is rooted in the concept of model-induced dependences between input and output (e.g., $\delta_{\Theta_n} = 0$ if Θ_n and *Y* are uncorrelated), similar to I_{Θ_n} and $I^*_{\Theta_n}$. Whereas dependences in the former are defined in the (θ_n, Y) space, the latter considers the $(F_{\Theta_n}(\theta_n), F_Y(y))$ space. Otherwise, we note that δ_{Θ_n} is a global sensitivity index w.r.t. both the input and the output and focuses on the averaged value of the sensitivity metric, while not being conducive to capturing possible variations of the latter as a function of either Θ_n or *Y*. As such, indices δ_{Θ_n}, I_{Θ_n} and $I^*_{\Theta_n}$ are not overlapping and can be employed in conjunction for a comprehensive characterization of input-output sensitivity.

3. Examples of Applications

This section is devoted to the exemplification of the GSA methodology illustrated in Section 2 to provide evidence of its added value with respect to traditional GSA approaches. We do so through three simplified models, corresponding to an analytical test function, and two scenarios previously presented in the literature and related to flow and transport in porous media. These correspond to a setting representing pumping in a coastal aquifer and a laboratory-scale solute transport experiment within a heterogeneous porous medium. These examples enable us to clearly document the salient features and capabilities of the GSA approach we present.

While applications of our GSA methodology to scenarios of flow and transport in porous media characterized by an increased level of complexity will be considered in future studies, we recall that a possible constrain to the efficiency of our (as well as any other) GSA methodology could be related to computational issues. These are expected to pose some constraints depending on the interplay between (*a*) the degree of complexity of the physical setting analyzed, and/or (*b*) the number of uncertain model input parameters considered. As such, in some cases the development of a reduced-complexity (or surrogate) model might be required to represent the relationship between uncertain model input(s) and modeling goals at an affordable cost.

Evaluation of the bivariate copula density, $c(F_{\Theta_n}(\theta_n), F_Y(y))$, relies on the following steps. We start by drawing (within the input parameter space) a set of Monte Carlo samples at which the output of interest is evaluated through the model considered. The two-dimensional space $(F_{\Theta_n}(\theta_n), F_Y(y))$ is then populated and the associated numerical bivariate copula density is evaluated through a kernel density estimator. Here, we employ the diffusion-kernel method of Botev et al. (2010) which provides high quality results at affordable computational costs, other methodologies being fully compatible with our framework of analysis. We note that an analytical formulation for the bivariate copula could also be employed, given that the input-output dependences induced by the model are satisfactorily captured. Once the bivariate copula density is evaluated, indices I_{Θ_n} and $I^*_{\Theta_n}$ can be readily computed through (4)-(6). For completeness, in Appendix B we also evaluate diverse GSA indices for the three models we consider and illustrate in the following. Results for each of these models are grounded on a set of 10^6 Monte Carlo samples.

3.1. Analytical Test Function

As a first illustrative example, we focus on the following analytical test model

$$Y = \begin{cases} X_1 + X_2 & if \;\; X_1 + X_2 \le 1 \\ 1 + X_3 & if \;\; X_1 + X_2 > 1 \end{cases}, \tag{7}$$

(X_1, X_2, X_3) being independent random variables uniformly distributed within the support [0,1]. We choose model (7) in light of its simplicity and to exemplify our methodology in the case where an input-output copula exhibits singular components, i.e., the bivariate copula between $F_{X_3}(x_3)$ and $F_Y(y)$ in this setting. Note that, according to (7), $c(F_{X_1}(x_1), F_Y(y)) = c(F_{X_2}(x_2), F_Y(y))$, and therefore $I_{X_1} = I_{X_2}$, $I^*_{X_1} = I^*_{X_2}$.

Fig. 1 depicts (*a*) I_{X_i} (with i = 1, 2, 3) versus $F_Y(y)$; (*b*) $F_Y(y)$ versus *y*; (*c*) $I^*_{X_i}$ versus $F_Y(y)$; (*d*) the empirical copula densities $c(F_{X_1}(x_1), F_Y(y))$; (*e*) the sensitivity descriptor $\left|1 - c(F_{X_1}(x_1), F_Y(y))\right|$ versus $F_{X_1}(x_1)$ for three selected value of $F_Y(y)$; and (*f*) the scatter plot of Grade(x_3) versus Grade(*y*).

The structure of model (7) reveals that *Y* does not depend on X_3 when $Y \le 1$. This observation is supported by joint inspection of Fig. 1*b*, which reveals that $F_Y(y = 1) = 0.5$, and of Fig. 1*f*, which indicates that values of Grade(*y*) ≤ 0.5 (i.e., $Y \le 1$) are independent from Grade(x_3). Otherwise, when Grade(*y*) ≥ 0.5 (i.e., *Y* > 1) there is a one-to-one correspondence between values of Grade(*y*) and Grade(x_3) (i.e., between *Y* and X_3), as expected from the structure of model (7). This means that the copula between $F_Y(y)$ and $F_{X_3}(x_3)$ exhibits singular components for $F_Y(y) > 0.5$. These observations lead us to conclude that $I_{X_3}(F_Y(y) \le 0.5) = 0$ and $I_{X_3}(F_Y(y) > 0.5) = 1$ as displayed by Fig. 1*a*, i.e., *Y* values associated with $F_Y(y) \le 0.5$ are not sensitive to X_3, while the ensuing values of *Y* associated with $F_Y(y) > 0.5$ depend solely on X_3. At the same time, it is possible to recognize that $I^*_{X_3}(F_Y(y) \le 0.5) = 0$ and $I^*_{X_3}(F_Y(y) > 0.5) = 1$ (see Fig. 1*c*), i.e., *Y* values associated with $F_Y(y) \le 0.5$ have a uniform level of (null) sensitivity to X_3 while the level of inhomogeneity in the sensitivity of each $Y > 1$ (i.e., $F_Y(y) > 0.5$) across the range of X_3 is largest, because model (7) induces a one-to-one correspondence between X_3 (i.e., $F_{X_3}(x_3)$) and $Y > 1$ (i.e., $F_Y(y) > 0.5$). We underline that our numerical evaluation of $c(F_{X_3}(x_3), F_Y(y))$ is in agreement with its theoretical counterpart (i.e., for $F_Y(y) \le 0.5$, $c(F_{X_3}(x_3), F_Y(y)) = 1 \;\; \forall F_{X_3}(x_3)$; and for $F_Y(y) > 0.5$, $c(F_{X_3}(x_3), F_Y(y)) \to \infty$ for $F_{X_3}(x_3) = 2F_Y(y) - 1$, while $c(F_{X_3}(x_3), F_Y(y)) = 0$ elsewhere), despite the challenges posed by the numerical evaluation of the singular components of the copula density in this case (details not shown). These findings provide further support to the robustness of the numerical procedure employed to estimate the empirical copula densities.

Inspection of Fig.s 1*a*, *c* reveals that indices I_{X_1} (and therefore I_{X_2}) and $I^*_{X_1}$ (and $I^*_{X_2}$) have a non-zero constant value for $F_Y(y) > 0.5$. This behavior descends from the observation that even as X_3 dictates the specific value of Y when $Y > 1$ (i.e., the value of $F_Y(y)$ for $F_Y(y) > 0.5$), the latter is sensitive to X_1 and X_2 (i.e., to $F_{X_1}(x_1)$ and $F_{X_2}(x_2)$) through the fulfillment of the condition $X_1 + X_2 > 1$ in (7). The constant value of I_{X_1} (or I_{X_2}) for all $F_Y(y) > 0.5$ stems from the threshold-nature of this condition, i.e., the values of Y associated with $F_Y(y) > 0.5$ are all equally sensitive to the fulfillment of the threshold condition in (7). The non-zero constant value of $I^*_{X_1}$ (or $I^*_{X_2}$) for $F_Y(y) > 0.5$ is related to the observation that the threshold condition is more easily satisfied for a high rather than for a low value of X_1 (or X_2) (i.e., the strength of the sensitivity of each $Y > 1$ varies across the support of X_1 (or X_2), see also Fig. 1*d* for $F_Y(y) > 0.5$).

The behavior of I_{X_1} and $I^*_{X_1}$ (as well as I_{X_2} and $I^*_{X_2}$) for $F_Y(y) \le 0.5$ is related to the admissible values of X_1 (or X_2) for which $Y \le 1$ is fulfilled. Model (7) dictates that values of both inputs X_1 and X_2 must be low to yield low values of Y (i.e., low $F_Y(y)$), this feature yielding a strong dependence only for few values of the inputs. As Y increases towards unity, I_{X_1} decreases because there is an increase of the number of values of X_1 that are compatible with the condition $Y \le 1$ (thus leading to a decreased strength of the dependence between specific value of Y and X_1, as also shown in Fig. 1*d*). At the same time, index $I^*_{X_1}$ first decreases (i.e., the sensitivity metric $\left|1 - c(F_{X_1}(x_1), F_Y(y))\right|$ becomes more uniform across the whole range of X_1 values), and then increase until $F_Y(y) = 0.3$, to then decrease again upon approaching $F_Y(y) = 0.5$. This behavior stems from the fact that, as $F_Y(y)$ increases (from 0 to 0.5) the copula density $c(F_{X_1}(x_1), F_Y(y))$ (*i*) is larger than zero for a widening range of $F_{X_1}(x_1)$ values. At the same time, $c(F_{X_1}(x_1), F_Y(y))$ (*i*) is independent of $F_{X_1}(x_1)$ for a given $0.0 \le F_Y(y) \le 0.5$ and (*ii*) decreases monotonically towards 1.0 as $F_Y(y)$ approaches 0.5. This aspect is further elucidated by Fig. 1*e*, showing that the variability of the descriptor $\left|1 - c(F_{X_1}(x_1), F_Y(y))\right|$ around its mean value does not monotonically increase/decrease with $F_Y(y)$.

3.2 Critical Pumping Rate in a Coastal Aquifer

We consider here the critical pumping rate (Q_c') that can be extracted from a fully penetrating pumping well operating in a homogenous confined coastal aquifer of uniform thickness (b') to ensure that a concentration of dissolved salt not exceeding 1% is detected at the well. The well is placed at a distance X_w' from the coastline and a constant freshwater flux (q_f') is flowing from the inland to the coastline. The (dimensionless) critical pumping rate ($Q_c = Q_c' / (b' X_w' q_f')$) can then be approximated through (Pool and Carrera, 2011)

$$\lambda_D = 2\left[1 - \frac{Q_c}{\pi}\right]^{1/2} + \frac{Q_c}{\pi}\ln\frac{1-(1-Q_c/\pi)^{1/2}}{1+(1-Q_c/\pi)^{1/2}} \qquad \text{with} \qquad \lambda_D = \frac{\Delta\rho'}{\rho_f'}\frac{1-(PE_T)^{-1/6}}{X_w J}, \tag{8}$$

where $X_w = X_w' / b'$; $J = q_f' / K'$; $PE_T = b' / \alpha_T'$; K' is the hydraulic conductivity of the aquifer; α_T' is transverse dispersivitiy; $\Delta\rho' = \rho_s' - \rho_f'$, ρ_f' and ρ_s' being the density of freshwater and saltwater, respectively. Note that (8) has been derived in the range of $\lambda_D \in [0-10]$. Further details about the problem setting, boundary and initial conditions, as well as geometrical configuration of the system, can be found in Pool and Carrera (2011).

Our scope here is to investigate the results of our copula density-based GSA for Q_c. We consider $PE_T \in [0.01-0.1]$, $J \in [0.8-2.5]\times 10^{-3}$, and $X_w \in [10-33]$ as uncertain model parameters in (8). It should be noted that in practical applications the values of PE_T and *J* are difficult to assess experimentally, the variability in the well location being considered as an operational/design variable. The selected ranges of parameter uncertainty have also been used by Dell'Oca et al. (2017) in the context of their moment-based GSA and are designed to (*i*) resemble realistic field values and (*ii*) obey the above-mentioned constraint about λ_D.

Fig. 2 depicts (*a*) I_{Θ_n} (with Θ_n = PE_T, X_w, and *J*) versus $F_{Q_c}(q_c)$; (*b*) $F_{Q_c}(q_c)$ versus q_c; (*c*) $I^*_{\Theta_n}$ versus $F_{Q_c}(q_c)$; and the empirical copula densities (*d*) $c(F_{PE_T}(pe_T), F_{Q_c}(q_c))$, (*e*) $c(F_{X_w}(x_w), F_{Q_c}(q_c))$, and (*f*) $c(F_J(j), F_{Q_c}(q_c))$. Fig.s 2*a*, *c* show that $I_J \approx I_{X_w}$ and $I^*_J \approx I^*_{X_w}$ for any value of $F_{Q_c}(q_c)$. This result is consistent with (*i*) the format of (8), showing that Q_c varies in the same (nonlinear) way due to variability of X_w or *J*, and (*ii*) the adoption of a very similar coefficient of variation for both X_w and *J* (≈ 0.31 and 0.30 for X_w and *J*, respectively.). A similar reasoning underpins the observation that $c(F_J(j), F_{Q_c}(q_c)) \approx c(F_{X_w}(x_w), F_{Q_c}(q_c))$ (see Fig.s 2*e*,*f*). It is also noted that the sensitivity of the intermediate values of $F_{Q_c}(q_c)$ is less intense (i.e., with reduced values for I_J and I_{X_w}) and more uniform with respect to either $F_J(j)$ or $F_{X_w}(x_w)$ (note the low values of I^*_J and $I^*_{X_w}$) as compared to the behavior displayed for high and low values of $F_{Q_c}(q_c)$. As an additional result, we note that $I_{PE_T} < I_J$ (or I_{X_w}), and $I^*_{PE_T} < I^*_J$ (or $I^*_{X_w}$) for all $F_{Q_c}(q_c)$, i.e., the sensitivity of each $F_{Q_c}(q_c)$ to $F_{PE_T}(pe_T)$ is always less strong and more uniform than its counterpart associated with $F_J(j)$ or $F_{X_w}(x_w)$ despite the large coefficient of variation adopted for PE_T (≈ 0.47). This result is due to the format of the model employed (8). Finally, it is also worth noting that values of indices I_{PE_T} and $I^*_{PE_T}$ are highest for $F_{Q_c}(q_c) \to 0$, such values being quite close to their counterparts associated with $F_J(j)$ and $F_{X_w}(x_w)$. This aspect is linked to the high intensity of $c(F_{PE_T}(pe_T), F_{Q_c}(q_c))$ for low $F_{PE_T}(pe_T)$ (see Fig. 2*d*).

Our results are consistent with an interpretation of the system behavior according to which the intensity of the dispersion mechanism does not play a marked role in comparison to the role of *J* and X_w when high values of the pumping rate at the well can be extracted. This observation is in agreement with the intuition that high values of pumping flow rate are allowed only when the intensity of the incoming freshwater, the overall thickness of the system and/or the well distance from the coast are sufficiently high to hamper well contamination, despite the level of transverse dispersion of the dissolved salt. Otherwise, the strength of the transverse dispersive mechanism becomes a relevant factor, together with J and X_w, for low values of Q_c. This result is consistent with the observation that there can be an enhanced well contamination in case of high level of (dimensionless) solute dispersion (i.e., very low PE_T), low (dimensionless) incoming freshwater flux, and for well locations that are relatively close to the coastline.

Outcomes of the copula-based SA illustrated above are in line with the findings of Dell'Oca et al. (2017). These authors grounded their analysis on a moment-based GSA, which revealed that the first four statistical moments of the *pdf* of Q_c are mostly equally sensitive to J and X_w, a diminished sensitivity being displayed with respect to PE_T. Otherwise, the added value of the results stemming from the copula-based SA lies in the characterization of the sensitivity of Q_c across its entire range of values, supporting enhanced understanding of the way model (8) drives the relationship between inputs (i.e., J, X_w and PE_T) and output of interest (i.e., Q_c).

3.3 Laboratory-scale solute transport within a heterogeneous porous medium

We consider the laboratory-scale setting illustrated by Esfandiar et al. (2015). These authors analyze the results of a solute transport experiment performed within a rectangular flow cell filled with two distinct uniform materials, i.e., a coarse and a fine sand. A sketch of the experimental setup and of the geometrical arrangement of the two types of sand employed in the experiment is depicted in Fig. 3*a*. A unit step injection of a non-reactive solute is imposed at the inlet of the flow cell, within which a steady-state strongly nonuniform flow takes place. The temporal evolution of solute concentration at the flow cell outlet (normalized by the concentration of the injected solution), i.e., $\overline{C}(t)$, t being time, is measured. Esfandiar et al. (2015) model $\overline{C}(t)$ by numerically solving the classical advection-dispersion equation within the porous domain, employing an efficient space-time grid adaptation strategy. The authors consider longitudinal dispersivities (i.e., α_{L_i} with $i = 1, 2$ for the coarse and fine sand, respectively) of the sands as uncertain system parameters to be estimated against the experimental breakthrough curve. In order to reduce the computational burden of the model calibration procedure, Esfandiar et al. (2015) rely on a representation of $\overline{C}(t)$ through a generalized Polynomial Chaos Expansion (gPCE) as a surrogate model (see Appendix A), considering the $\log_{10}\left(\alpha_{L_i}\right)$ (with $i = 1, 2$) as two indipendent random variables, uniformly distributed within the support [-6, -2]. Here, we leverage on the gPCE representation of Esfandiar et al. (2015) and assess the sensitivity of $\overline{C}(t)$ with respect to $\log_{10}\left(\alpha_{L_i}\right)$ according to the methodology detailed in Section 2.

Fig. 3*b* depicts the time evolution of a collection of 100 samples (grey curves; randomly selected from the 10^6 Monte Carlo realizations) of $\overline{C}(t)$ at the outlet of the system and the ensuing expected value, i.e., $E\left[\overline{C}(t)\right]$ (black curve). The narrowing of the spread of the Monte Carlo realizations at times corresponding to $E\left[\overline{C}(t)\right] \approx 0.4$ suggests that $\overline{C}(t)$ is mainly controlled by the intensity of advective processes (here considered as deterministic) at such times (i.e., the deterministic advective transport component is a key driver of the displacement of the center of mass of the solute plume). Otherwise, the behavior of $\overline{C}(t)$ at earlier and later times is tied to the intensity of the dispersion processes within the coarse and fine material (i.e., to α_{L_1} and α_{L_2}, respectively), as further discussed in the following.

Fig. 4 depicts a color scale representation of $I_{\log_{10}\left(\alpha_{L_i}\right)}$ (*a*, *b*) and $I^{*}_{\log_{10}\left(\alpha_{L_i}\right)}$ (*c*, *d*) against $F_{\overline{C}(t)}(\overline{c}(t))$ and $E\left[\overline{C}(t)\right]$. Note that we plot results against $E\left[\overline{C}(t)\right]$ rather than time *t*, for ease of interpretation of outcomes (see our discussion of Fig. 3b).

Joint inspection of Fig.s 4*a*, *b* indicates that at early breakthrough times (i.e., $E\left[\overline{C}(t)\right] < 0.2$ approximately) $I_{\log_{10}\left(\alpha_{L_1}\right)}$ is larger than $I_{\log_{10}\left(\alpha_{L_2}\right)}$ for all $F_{\overline{C}(t)}(\overline{c}(t))$ values. This result supports a major importance of α_{L_1} (as opposed to α_{L_2}) for early times and is linked to the observation that at these times the solute has traveled primarily through the coarse sand, which resides in the largest portion of the domain. Considering such a strong sensitivity of the solute concentration at the outlet (in the presence of a material characterized by α_{L_2}) to α_{L_1}, is also consistent with a non-locality of the transport mechanism within the heterogenous system under investigation (i.e., solute concentration at a given point is influenced by the system properties at other locations). The relevance of the coarse medium dispersivity is also documented through inspection of Fig. 4*c* where high values of $I^{*}_{\log_{10}\left(\alpha_{L_1}\right)}$ are seen for $E\left[\overline{C}(t)\right] < 0.2$ (approximately) across all $F_{\overline{C}(t)}(\overline{c}(t))$, i.e., the bivariate copula densities (see Fig. SM1a) exhibit high values for each $F_{\overline{C}(t)}(\overline{c}(t))$ within a narrow range of values of α_{L_1}, suggesting a nearly one-to-one correspondence between the former and the latter. Yet, inspection of Fig.s 4*a*-*d* reveal that the output $\overline{C}(t)$ at early times (i.e., for $E\left[\overline{C}(t)\right] < 0.2$) tends to be equally sensitive (in terms of $I_{\log_{10}\left(\alpha_{L_i}\right)}$ and $I^{*}_{\log_{10}\left(\alpha_{L_i}\right)}$) to the dispersivities of both materials in the range $0.4 < F_{\overline{C}(t)}(\overline{c}(t)) < 0.6$ (i.e., within the latter range the ensuing value of $\overline{C}(t)$ is governed by the intensity of the dispersive process within both materials). Otherwise, low and high values of $F_{\overline{C}(t)}(\overline{c}(t))$ are more sensitive to the value of the dispersivity of the coarse sand (across which the solute tends to travel/spread the most).

Focusing on the range $0.2 < E\left[\overline{C}(t)\right] < 0.4$, inspection of Fig.s 4*a*, *b* suggests an equal importance of both α_{L_1} and α_{L_2}, the former and the latter displaying a strong dependence on the high and low values of $F_{\overline{C}(t)}(\overline{c}(t))$, respectively. At the same time, Fig.s 4*c*, *d* document that in this setting high values for $I^{*}_{\log_{10}\left(\alpha_{L_1}\right)}$ and $I^{*}_{\log_{10}\left(\alpha_{L_2}\right)}$ correspond to high values of $I_{\log_{10}\left(\alpha_{L_1}\right)}$ and $I_{\log_{10}\left(\alpha_{L_2}\right)}$. These observations suggest that the dispersivities of both materials affect $\overline{C}(t)$ before the arrival of the plume center of mass. This result descends from the observation that an increasing amount of solute has traveled through the coarse medium and is conveyed through the fine material at these times, thus yielding an increased relevance of the intensity of the dispersion process within the fine material. We note that the high values of $I_{\log_{10}\left(\alpha_{L_1}\right)}$ (and of $I^{*}_{\log_{10}\left(\alpha_{L_1}\right)}$) corresponding to high $F_{\overline{C}(t)}(\overline{c}(t))$ are due to a strong dependence of $F_{\overline{C}(t)}(\overline{c}(t))$ on low values of α_{L_1} (see Fig. SM1c), i.e., high values of $\overline{C}(t)$ are associated with a relatively low dispersion of the plume as it migrates across the coarse material, resulting in a less diluted plume at the outlet. On the other hand, the high values of $I_{\log_{10}(\alpha_{L_2})}$ (and of $I^*_{\log_{10}(\alpha_{L_2})}$) corresponding to low $F_{\overline{C}(t)}(\overline{c}(t))$ are associated with a strong dependence between $F_{\overline{C}(t)}(\overline{c}(t))$ and high values of α_{L_2} (see Fig. SM1d), i.e., an intense dispersion of the plume within the fine material is key to lead to relatively low $\overline{C}(t)$.

Considering $E\left[\overline{C}(t)\right] > 0.4$, Fig.s 4*a*, *b* highlights that, overall, $I_{\log_{10}(\alpha_{L_2})}$ tends to increase with $E\left[\overline{C}(t)\right]$ (this is especially evident for the lowest values of $F_{\overline{C}(t)}(\overline{c}(t))$, see previous discussion). Otherwise, $I_{\log_{10}(\alpha_{L_1})}$ tends to decrease with $E\left[\overline{C}(t)\right]$, with the exception of the region of high values of $F_{\overline{C}(t)}(\overline{c}(t))$, i.e., $F_{\overline{C}(t)}(\overline{c}(t)) > 0.9$ (approximately), and for $0.2 < F_{\overline{C}(t)}(\overline{c}(t)) < 0.5$ (approximately). We note that the high values of $I_{\log_{10}(\alpha_{L_2})}$ ($I_{\log_{10}(\alpha_{L_1})}$) and of $I^*_{\log_{10}(\alpha_{L_2})}$ ($I^*_{\log_{10}(\alpha_{L_1})}$) corresponding to low (high) $F_{\overline{C}(t)}(\overline{c}(t))$ are due to a strong dependence of $F_{\overline{C}(t)}(\overline{c}(t))$ on low (high) values of α_{L_2} (α_{L_1}), as also seen in Fig. SM1*f* and SM1*e*, respectively. This finding may reflect the tendency (at late times) to hinder (enhance) solute entering from the coarse to the fine medium and to subsequently being transported through it, as the dispersivity of the fine (coarse) medium decreases (increases). These results are in agreement with the observation that the intensity of the dispersion process in the fine material becomes the most relevant factor determining the monitored concentration at the outlet as time increases, even as the highest values of concentration still show some dependency on the dispersivity of the coarse medium (see previous discussion about non-locality of transport).

The width of the two segments of $F_{\overline{C}(t)}(\overline{c}(t))$ values (approximately corresponding to $F_{\overline{C}(t)}(\overline{c}(t)) > 0.9$ and $0.2 < F_{\overline{C}(t)}(\overline{c}(t)) < 0.5$) associated with large $I_{\log_{10}(\alpha_{L_1})}$ values tends to narrow as time increases. This behavior can be linked to the loss of memory of solute transport dynamics with respect to the influence of dispersive properties of the coarse sand region as the intensity of the dispersion process in the second material gain relevance (see also Dell'Oca et al., 2019). At the same time, Fig. 4*d* reveals that $I^*_{\log_{10}(\alpha_{L_2})}$ is quite strong across the entire range of $F_{\overline{C}(t)}\left(\overline{c}(t)\right)$ (with the exception of very high values of the latter), suggesting that there is a direct correspondence between a given value of $\overline{C}(t)$ and α_{L_2} (see Fig. SM1*f*). A similar feature is suggested by inspection of Fig. 4*c*, where one can observe that $I^*_{\log_{10}(\alpha_{L_1})}$ is high within the regions $0.2 < F_{\overline{C}(t)}(\overline{c}(t)) < 0.5$ (approximately) and $F_{\overline{C}(t)}(\overline{c}(t)) > 0.9$, whereas the analysis of bivariate copula (see Fig. SM1*e*) indicates intense values of the copula density for intermediate and high values of α_{L_1} when $0.2 < F_{\overline{C}(t)}(\overline{c}(t)) < 0.5$ or $F_{\overline{C}(t)}(\overline{c}(t)) > 0.9$, respectively.

The main findings provided by the application of our copula-based SA to this laboratory-scale solute transport scenario are in overall agreement with the moment-based GSA illustrated by Dell'Oca et al. (2017), i.e., the sensitivity of $\overline{C}(t)$ to the dispersivity of the fine material tends to increase with time, while the influence of the dispersivity of the coarse material decreases. Moreover, assisting GSA through our copula-based analysis has the added value of providing a quantitative characterization of the nature of the ensuing sensitivity across the entire range of $F_{\overline{C}(t)}(\overline{c}(t))$ values, thus linking our understanding of the system functioning to the documented features of the sensitivity of $\overline{C}(t)$ to the dispersivities of the two materials.

4. Conclusions

We propose an original approach to Sensitivity Analysis which is Global with respect to the model input(s) and Local with respect to the model output, i.e., it enables one to characterize sensitivity for each of the possible values undertaken by the model output of interest. In this sense, one can then quantify the influence of model uncertain parameters on the quantiles of the distribution of the modeling goal of interest.

At the hearth of our methodology there is the copula density between selected model input and the targeted output. As a descriptor for sensitivity, we select the absolute distance between such copula density and its counterpart associated with two independent random variables. We then characterize the sensitivity of a model output locally (i.e., for each possible value of the output) with respect to an uncertain input by relying on two indices, each summarizing a global behavior (with respect to the variability of the input) of sensitivity. Specifically, we evaluate (*i*) the averaged (across all values of an input, i.e., globally) value and (*ii*) the degree of variability (across all values of an input, i.e., again globally) of the introduced sensitivity descriptor.

Relying on the copula density enables one to assess model-induced dependences at any order (i.e., without being limited to linear dependences) among a model input and a given modeling output, independent from the marginal behavior of the latter. As opposed to typically employed GSA approaches, where one evaluates the importance of a model input to an output through summary indices, our copula density technique enables one to quantify the sensitivity of a model input to the entire range of the quantiles of the distribution of the output. This aspect is particular critical in risk assessment procedures, allowing to quantify the impact of a given model parameter for low or high values of the output of interest (as seen, e.g., with reference to a well pumping rate or the temporal behavior of solute concentrations), or if there are regions (or values) in the space of variability of the output that are not influenced by one or more model inputs. As such, our copula density Sensitivity Analysis can contribute to enhance our ability to diagnose the functioning of a given model.

We provide evidence of the type of information that our approach ensures by focusing on an analytical test function, on a setting associated with the determination of the critical pumping rate at a well placed in a coastal aquifer, and on a laboratory-scale solute transport experiment performed within a heterogeneous porous medium.

Acknowledgements

The authors would like to thank the EU and MIUR for funding, in the frame of the collaborative international Consortium (WE-NEED) financed under the ERA-NET WaterWorks2014 Cofunded Call. This ERA-NET is an integral part of the 2015 Joint Activities developed by theWater Challenges for a Changing World Joint Programme Initiative (Water JPI).Part of the work was developed while Prof. A. Guadagnini was at the University of Strasbourg with funding from Région Grand-Est and Strasbourg-Eurométropole through the 'Chair Gutenberg'.

References

Bárdossy, A., 2006. Copula-based geostatistical models for groundwater quality parameters. Water Resour. Res. 42 (11), W11416. https://doi.org/10.1029/2005WR004754.

Borgonovo, E., 2007. A new uncertainty importance measure. Reliab. Eng. Syst. Saf. 92 (6), 771-784. https://doi.org/10.1016/j.ress.2006.04.015.

Borgonovo, E., Hazen, G. B., Plischke, E., 2016. A common rationale for global sensitivity measures and their estimation. Risk Analysis, 36(10), 1871-1895. https://doi.org/10.1111/risa.12555

Botev, Z. I., Grotowski, J. F., Kroese, D. P., 2010. Kernel density estimation via diffusion. A. of Statist 38 (5), 2916-2957.

Campolongo, F., Saltelli, A., Cariboni, J., 2013. From screening to quantitative sensitivity analysisi. A unified approach. Comp. Phys. Commun. 182(4), 978-988. https://doi.org/10.1016/j.cpc.2010.12.039

Ceriotti, G., Russian, A., Bolster, D., Porta, G., 2019. A double-continuum transport model for segregated porous media: Derivation and sensitivity analysis-driven calibration. Adv. Water Resour. 128, 206-217. https://doi.org/10.1016/j.advwatres.2019.04.003

Chang, Y., Li, Y., Ding, A. A., Dy, J. G., 2016. A robust-equitable Copula dependence measure for feature selection. Proceedings of the 19th International Conference on Artificial Intelligence and Statistics (AISTATS), Cadiz, Spain. JMLR: WCP volume 41.

Crick, M. J., Hill, M. D., Charles, D., 1987. The Role of Sensitivity Analysis in Assessing Uncertainty. Proceedings of an NEA Workshop on Uncertainty Analysis for Performance Assessments of Radioactive Waste Disposal Systems, Paris, pp. 1-258.

Da Veiga, S., 2015. Global sensitivity analysis with dependence measures. J. Statist. Comp. Sim., 85(7), 1283-1305. https://doi.org/10.1080/00949655.2014.945932

De Lozzo, M., Marrel, A., 2016. New improvements in the use of dependence measures for sensitivity analysis and screening. J. Statist. Comp. Sim. 86(15), 3038-3058. https://doi.org/10.1080/00949655.2016.1149854

Delfs, J.-O., Park, C.-H., Kolditz, O., 2009. A sensitivity analysis of Hortonian flow. Adv. Water Resour. 32(9), 1386-1395. https://doi.org/10.1016/j.advwatres.2009.06.005

Dell'Oca, A., Riva, M., Guadagnini, A., 2017. Moment-based metrics for global sensitivity analysis of hydrological systems. Hydr. Earth Syst. Sci. 21, 6219-6234. https://doi.org/10.5194/hess-21-6219-2017

Dell'Oca, A., G. Porta, A. Guadagnini, M. Riva, 2018. Space-time mesh adaptation for solute transport in randomly heterogeneous porous media. J. Contam. Hydrol. 2012, 28-40, doi:http://dx.doi.org/10.1016/j.jconhyd.2017.07.001

Dell'Oca, A., M. Riva, P. Ackerer, A. Guadagnini, 2019. Solute transport in random composite media with uncertain dispersivities. Adv. Water Resour. 128, 48-58. doi:10.1016/j.advwatres.2019.04.005

Di Fusco, E., Lauriola, I., Verdone, R., Di Federico, V., Ciriello, V., 2018. Impact of uncertainty in soil texture parameters on estimation of soil moisture through radio waves transmission. Adv. Water Resour. 122, 131-138. https://doi.org/10.1016/j.advwatres.2018.10.007

Di Palma, P. R., Guyennon, N., Heβe, F., Romano, E., 2017. Porous media flux sensitivity to pore-scale geostatistics: A bottom-up approach. Adv. Water Resour. 102, 99-110. https://doi.org/10.1016/j.advwatres.2017.02.002

Durante, F., Fernández-Sánchez, J., Sempi, C., 2013. A note on the notion of singular copula. Fuzzy Sets Syst. 211 (16), 120-122. https://doi.org/10.1016/j.fss.2012.04.005.

Esfandiar, B., Porta, G., Perotto, S., Guadagnini, A., 2015. Impact of space-time mesh adaptation on solute transport modeling in porous media. Water Resour. Res. 51, 1315-1332, doi:10.1002/2014WR016569.

Formaggia, L., Guadagnini, A., Imperiali, I., Lever, V., Porta, G., Riva, M., Scotti, A., and Tamellini, L.: Global sensitivity analysis through polynomial chaos expansion of a basin-scale geochemical compaction model. Comput. Geosci., 17, 25-42, https://doi.org/10.1007/s10596-012-9311-5, 2013.

Gupta, H. V., Razavi, S., 2018. Revisiting the basis of sensitivity analysis of dynamical earth system model. Water Resour. Res. 54 (11), 8692-8717. https://doi.org/10.1029/2018WR022668

Hamby, D. M., 1994. A review of techniques for parameter sensitivity analysis of environmental models. Environ. Monit. Assess. 32 (2), 135-154. https://doi.org/10.1007/BF00547132

Krzykacz-Hausmann, B., 2001. Epistemic sensitivity analysis based on the concept of entropy. Proceedings of SAMO 2001, Madrid, pp. 31–35. CIEMAT.

Marino, S., Hogue, I. B., Ray, C. J., Kirschner, D. E., 2009. A methodology for performing global uncertainty and sensitivity analysis in systems biology. J. Theor. Biol. 254, 178-196. https://doi.org/10.1016/j.jtbi.2008.04.011

Morris, M., 1991. Factorial sampling plans for preliminary computational experiments. Technom. 33 (2), 161-174.

Most, S., Bijeljic, B., Nowak, W., 2016. Evolution and persistence of cross-directional statistical dependence during finite-Péclet transport through a real porous medium. Water Resour. Res. 52, 8920-8937. https://doi.org/10.1002/2016WR018969.

Nelsen, R. B., 2013. An Introduction to Copulas. Springer, New York, 139, pp. 1–272. doi:10.1007/0-387-28678-0.

Oladyshkin, S., de Barros, F. P. J., Nowak, W., 2012. Global sensitivity analysis: A flexible and efficient framework with an example from stochastic hydrogeology. Adv. Water Resour. 37, 10-22. https://doi.org/10.1016/j.advwatres.2011.11.001

Pianosi, F., Beven, K., Freer, J., Hall, J. W., Rougier, J., Stephenson, D. B., Wagener, T., 2016. Sensitivity analysis of environmental models: A systematic review with practical workflow. Environ. Model. Softw. 79, 214-232. http://dx.doi.org/10.1016/j.envsoft.2016.02.008

Pianosi, F., Wagener, T., 2015. A simple and efficient method for global sensitivity analysis based on cumulative distribution functions. Environ. Model. Softw. 67, 1–11. https://doi.org/10.1016/j.envsoft.2015.01.004.

Pool, M., Carrera, J., 2011. A correction factor to account for mixing in Ghyben-Herzberg and critical pumping rate approximations of seawater intrusion in coastal aquifers. Water Resour. Res. 47, W05506. https://doi.org/10.1029/2010WR010256

Porta, G., la Cecilia, D., Guadagnini, A., Maggi, F., 2018. Implications of uncertain bioreactive parameters on a complex reaction network of atrazine biodegradation in soil. Adv. Water Resour. 121, 263-276. https://doi.org/10.1016/j.advwatres.2018.08.002

Rakovec, O., Hill, M.C., Clark, M.P., Weerts, A.H., Teuling, A.J., Uijlenhoet, R., 2014. Distributed Evaluation of Local Sensitivity analysis (DELSA), with application to hydrologic models. Water Resour. Res. 50 (1), 409-426. https://doi.org/10.1002/2013WR014063

Razavi, S., Gupta, H. V., 2016. A new framework for comprehensive, robust, and efficient global sensitivity analysis: 1. Theory. Water Resour. Res. 52 (1), 423-439. https://doi.org/10.1002/2015WR017558

Razavi, S., Gupta, H. V., 2015. What do we mean by sensitivity analysis? The need for comprehensive characterization of "global" sensitivity in Earth and Environmental systems models. Water Resour. Res. 51, 3070–3092. https://doi.org/10.1002/2014WR016527, 2015.

Sklar, A., 1973. Random variables, joint distribution functions, and copulas. Kybernetika 9(6), 449-460.

Sklar, A., 1996. Random variables, distribution functions, and copulas – A personal look backward and forward. Distributions with Fixed Marginals and Related Topics, IMS Lecture Notes - Monograph Series Vol. 28, 1996

Sobol, I. M., 2001. Global sensitivity indices for nonlinear mathematical models and their Monte Carlo estimates. Math. Comput. Sim. 55, 271-280.

Sochala, P., Le Maître, O. P., 2013. Polynomial chaos expansion for subsurface flows with uncertain soil parameters. Adv. Water Resour. 62, 139-154. https://doi.org/10.1016/j.advwatres.2013.10.003

Sole-Mari, G., Bolster, D., Fernàndez-Garcia, D., Sanchez-Vila, X., 2019. Particle density estimation with grid-projected and boundary-corrected adaptive kernels. Adv. Water Res. 131, 103382. https://doi.org/10.1016/j.advwatres.2019.103382

Székely, G. J., Rizzo, M. L., Bakirov, N. K., 2007. Measuring and testing dependence by correlation of distances. Ann. Stat., 35, 2769-2794.

Tebes-Stevens, C. L., Vlochhi, A. J., 2000. Calculation of reaction parameter sensitivity coefficients in multicomponent subsurface transport models. Adv. Water Resour. 23(6), 591-611. https://doi.org/10.1016/S0309-1708(99)00054-8

van Werkhoven, K., Wagener, T., Reed, P., Tang, Y., 2009. Sensitivity-guided reduction of parametric dimensionality for multi-objective calibration of watershed models. Adv. Water Resour. 32(8), 1154-1169. https://doi.org/10.1016/j.advwatres.2009.03.002

Xiao, S., Lu, Z., Wang, P., 2018. Global sensitivity analysis based on distance correlation for structural systems with multivariate output. Engineer. Struct. 167, 74-83. https://doi.org/10.1016/j.engstruct.2018.04.027

Appendix A. Generalized Polynomial Chaos Expansion approximation of the solute breakthrough curve associated with the laboratory-scale solute transport experimental set-up.

In order to reduce the computational burden associated with the copula-based SA in Section 3.3, we leverage on the surrogate model of the (normalized) concentrations measured at the flow cell outlet (i.e., $\overline{C}(t)$) introduced by Esfandiar et al. (2015). These authors rely on the generalized Polynomial Chaos Expansion (gPCE) (see, e.g., Sochala and Le Maître, 2013 and reference therein) of $\overline{C}(t)$, which can be cast as

$$\overline{C}(t) \approx \sum_{j=1}^{N} \beta_j \psi_i \left(\log_{10}\left(\alpha_{L_1}\right), \log_{10}\left(\alpha_{L_2}\right)\right) \tag{A.1}$$

where β_j are the so-called polynomial coefficients, ψ_i is a set of multivariate Legendre polynomials and N is the total number of employed polynomials. Esfandiar et al. (2015) evaluate the coefficients β_j through a sparse-grid procedure (see, e.g., Formaggia et al., 2013). They rely on the *total degree* rule for the selection of the set of multivariate Legendre polynomials, the *total degree* being set equal to 3, which leads to $N = 69$.

Appendix B. Evaluation of density-based, Morris, and Sobol' indices

We consider the three settings introduced in Section 3 and, in addition to the results presented in Section 3, we also evaluate (*i*) the density-based δ_{Θ_n} index (Borgonovo, 2007; Borgonovo et al., 2016), (*ii*) the Morris indices $\mu^*_{\Theta_n}$ and σ_{Θ_n} (Morris, 1991), and (*c*) the principal Sobol' indices. A brief summary of the definitions of these global sensitivity metrics is included in the following.

The δ_{Θ_n} index is defined as (see also Section 2)

$$\delta_{\Theta_n} = \frac{1}{2} E_Y E_{\Theta_n}\left[\left|p_{\Theta_n}(\theta_n) p_Y(y) - p_{\Theta_n,Y}(\theta_n, y)\right|\right], \tag{B.1}$$

where $p_{\Theta_n,Y}(\theta_n, y)$ is the bivariate *pdf* between the input Θ_n and the output Y, $p_{\Theta_n}(\theta_n) p_Y(y)$ is its counterpart under the assumption that Θ_n and Y are independent, $E_{\Theta_n}[-]$ and $E_Y[-]$ denoting expectation w.r.t. Θ_n and Y, respectively.

The Morris index $\mu^*_{\Theta_n}$ is defined as

$$\mu^*_{\Theta_n} = \frac{1}{r}\sum_{j=1}^{r}\left|\Xi_{\Theta_n}\right|, \qquad \text{with} \qquad \Xi_{\Theta_n} = \frac{Y(\Theta_1^j,...,\Theta_n^j + \Delta_n^j,...\Theta_N^j) - Y(\Theta_1^j,...,\Theta_n,...\Theta_1^j)}{\Delta_n^j}, \tag{B.2}$$

where the so-called *elementary effects* (Ξ_{Θ_n}) represent approximations of the Y derivative w.r.t. Θ_n, evaluated relying on increment Δ_n^j for diverse values (i.e., r times) of the remaining model inputs and (see Pianosi et al., 2016 and reference therein for a review of strategies for the definition of the combinations of input parameters suited for the evaluation of $\mu^*_{\Theta_n}$). According to (B.2), a high average variation in the model output due to model input perturbations corresponds to a high $\mu^*_{\Theta_n}$ value.

The Morris index σ_{Θ_n} reads

$$\sigma_{\Theta_n} = \frac{1}{r}\sqrt{\sum_{j=1}^{r}\left(\Xi_{\Theta_n} - \mu^*_{\Theta_n}\right)^2} . \tag{B.3}$$

Higher values of σ_{Θ_n} correspond to higher nonlinearity effects. This can be due to either a non-linearity in the relationship between Y and Θ_n or to interactions among Θ_n and other model inputs.

Inspection of (B.2) and (B.3) suggests that in the Morris method the output-input sensitivity is characterized in terms of both (*i*) an average value and (*ii*) a measure of the variability of the selected sensitivity metric (i.e., Ξ_{Θ_n}). In the methodology introduced in Section 2, we follow a similar rationale in the definition of (4)-(6).

The principal Sobol' index is defined as

$$S_{\Theta_n} = \frac{E_{\Theta_n}\left[V - V\left[Y \mid \theta_n\right]\right]}{V}, \tag{B.4}$$

Here, V is the model output variance and $V(Y \mid \theta_n)$ is its counterpart conditional to a given value (θ_n) of the input Θ_n. Expression (B.4) serves as a measure of the (normalized) contribution to the output variance due to the variability in the input parameter Θ_n. In other words, the higher is the (average) reduction of the model output variance due to the knowledge of Θ_n, the higher is S_{Θ_n}. As such, in the Sobol' method the sensitivity (rendered through the metric $V - V\left[Y \mid \theta_n\right]$) is grounded on the behavior of the model output variability, as quantified through its variance. In this context, we note that the variance may be an incomplete descriptor of the output variability (see, e.g., Pianosi et al., 2016; Borgonovo et al., 2007; Dell'Oca et al., 2017).

A distinctive feature typically shared by all global sensitivity indices is an integration across the support of the model input and/or output, the information provided by each index being characterized by the quantity being subject to integration (i.e., the sensitivity metric). In this context, it is noted that the approaches listed above ground sensitivity on diverse descriptors. These encapsulate the level of dependence between uncertain model input and output through (*i*) the bivariate *pdf* in δ_{Θ_n}, (*ii*) variations of model output due to input variations in the Morris approach, or (*iii*) the contribution of an input variability to the output variance for the Sobol' index. All of these approaches thus introduce a set of scalar indices resting on diverse strategies. For example, the Morris approach focuses on the average value and on the standard deviation of the sensitivity metric, whereas the focus in the *pdf*-based methodology is solely on the average value. It is then of interest to analyze possible similarities/discrepancies between results quantifying/ranking parameter sensitivity with these approaches and corresponding results stemming from I_{Θ_n} (4) and $I^*_{\Theta_n}$ (6), while recalling that each index emphasizes a diverse aspect of the output sensitivity to model input(s).

The results reported in the following are based on the same 10^6 Monte Carlo realizations employed for the evaluation of the copula densities in Section 3. Morris indices are computed by setting $r = 800$ and following the scheme presented by Campolongo et al. (2011).

Considering the analytical test function introduced in Section 3.1, we obtain $\mu^*_{X_1} = \mu^*_{X_2} = 1.06$, $\mu^*_{X_3} = 0.445$ and $\sigma_{X_1} = \sigma_{X_2} = 1.22$, $\sigma_{X_3} = 0.498$. The ensuing values of $\mu^*_{\Theta_n}$ suggest that variations in X_1 and X_2 lead to larger variations in the value of the output than those induced by variations in X_3. Values of σ_{Θ_n} indicate of a stronger level of nonlinearity (due to parameters interaction, see (7)) in the relationship between Y and X_1 (or X_2) than between Y and X_3. Principal Sobol' indices are

$S_{X_1} = S_{X_2} = 0.38$ and $S_{X_3} = 0.09$, these results being conducive to an ordering of input parameter relevance similar to what resulting from the Morris indices. Interestingly, relying on the density-based index yields a diverse ordering of the parameter relevance, since $\delta_{X_1} = \delta_{X_2} = 0.61$ and $\delta_{X_3} = 1.01$. These latter results are in agreement with those depicted in Fig. 1*a*, where we observe that the area below I_{X_1} and I_{X_2} is smaller than its counterpart corresponding to I_{X_3}. The set of outcomes here summarized is a stark example of the recognized multifaceted nature of the concept of *sensitivity*. Therefore, diverse methodologies focused on differing aspects of the output-input(s) sensitivity should be jointly investigated. In this context, we remark that I_{Θ_n} and $I^*_{\Theta_n}$ serve our understanding of the sensitivity of model outputs to parameters across the full range of outputs variability.

Results for the scenario targeting the critical pumping rate in a coastal aquifer (see Section 3.2) are: $\delta_{PE_T} = 0.31$, $\delta_{X_w} = 0.64$ and $\delta_J = 0.57$; $\mu^*_{PE_T} = 0.44$, $\mu^*_{X_w} = 1.01$, $\mu^*_J = 0.93$ and $\sigma_{PE_T} = 0.17$, $\sigma_{X_w} = 0.21$, $\sigma_J = 0.20$; and $S_{PE_T} = 0.09$, $S_{X_w} = 0.48$ and $S_J = 0.41$. On the basis of this set of results and those illustrated in Section 3.2, one can note a consistency in the way the relevance of the uncertain model inputs is rendered across the diverse Sensitivity Analysis methodologies, each with its own distinctive metric and specific aims. All of the results reveal that the critical pumping rate tends to be more sensitive to X_w, slightly less to J, and only to a minor extent to PE_T

With reference to the laboratory-scale solute transport scenario, Fig. B1 depicts (*a*) $\delta_{\log_{10}(\alpha_{Li})}$, (*b*) $\mu^*_{\log_{10}(\alpha_{Li})}$ and (*c*) $\sigma_{\log_{10}(\alpha_{Li})}$, as well as (*d*) $S_{\log_{10}(\alpha_{Li})}$ versus $E\left[\overline{C}(t)\right]$ for *i* = (1, 2) (blue and red curves, respectively). Overall inspection of Fig. B1 reveals that: (*i*) $\overline{C}(t)$ is more sensitive to the dispersivity of the coarse sand for $E\left[\overline{C}(t)\right] < 0.4$ (approximately); (*ii*) for values $E\left[\overline{C}(t)\right] \approx 0.4$, $\overline{C}(t)$ has a similar relative sensitivity to the dispersivities of the two sands; (*iii*) for $E\left[\overline{C}(t)\right] > 0.4$ the sensitivity of $\overline{C}(t)$ to the dispersivity of the fine sand is larger than that associated with the coarse sand (an exception is noted for $\delta_{\log_{10}(\alpha_{Li})}$, approximately within the range $0.5 < E\left[\overline{C}(t)\right] < 0.7$). It is here of interest to note that $\delta_{\log_{10}(\alpha_{L2})}$ and $S_{\log_{10}(\alpha_{L2})}$ tend to increase with $E\left[\overline{C}(t)\right]$, $\delta_{\log_{10}(\alpha_{L1})}$ and $S_{\log_{10}(\alpha_{L1})}$ being characterized by the opposite behavior. These results are in line with those discussed in Section 3.3 for our copula-based indices. Indices $\mu^*_{\log_{10}(\alpha_{Li})}$ and $\sigma_{\log_{10}(\alpha_{Li})}$ $(i = 1, 2)$ exhibit a bimodal behavior (the two peaks respectively occurring at $E\left[\overline{C}(t)\right] \approx 0.15$ and $E\left[\overline{C}(t)\right] \approx 0.70$) and display a decreasing trend for (approximately) $0.70 < E\left[\overline{C}(t)\right] < 1$, with similar values for *i* = 1 or 2. This set of results contributes to further highlight the different nature of the various sensitivity indices analyzed.

While the comparison of diverse methodologies here illustrated might not be exhaustive, it clearly documents how diverse strategies are keyed to diverse aspects of the output *sensitivity*. In this context, we recall that the copula-density based indices we propose are tied to the unique feature of detailing the output sensitivity across its range of variability (in terms of $F_Y(y)$).

With reference to the computational costs associated with the evaluation of the various indices here analyzed, we found that the *pdf*- and copula density-based analyses require a number of Monte Carlo iterations of the order of 10^5 to obtain stable results (in our computational examples we used a collection of 10^6 samples), while 10^4 and 10^3 realizations can be sufficient for the Sobol' and Morris indices, respectively. As a side remark, we note that we rely here on a straightforward Monte Carlo sampling for the evaluation of the *pdf*-based, copula density-based and Sobol' indices, while we use the strategy of Campolongo et al. (2011) for the Morris indices. It is then important to note that a variety of sampling strategies have been developed to reduce computational costs associated with the evaluation of the Morris, Sobol', and *pdf*-based (see e.g., Pianosi et al., 2016 and reference therein) indices. In this context, a future study will explore the possibility of employing an adaptive kernel estimation method (such as the one proposed by Sole-Mari et al., 2019) for the estimation of the model induced empirical copula density.

Figures

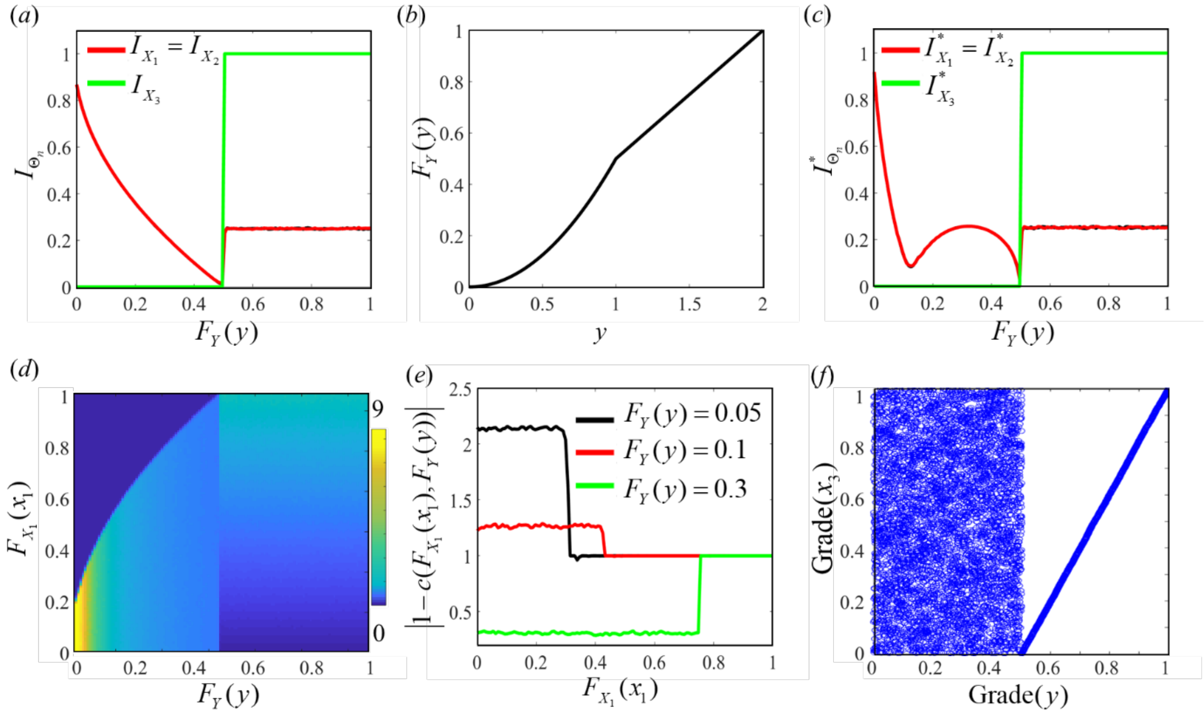

Fig. 1. Results of the Copula-density GSA for the output, i.e., Y, of the analytical test function in (7): (a) I_{Θ_n} and (c) $I^*_{\Theta_n}$ for Θ_n = X_1, X_2, X_3 against $F_Y(y)$; (b) $F_Y(y)$ versus y; (d) copula-density between $F_Y(y)$ and $F_{X_1}(x_1)$; (e) sensitivity descriptor $|1-c(F_{X_1}(x_1),F_Y(y))|$ versus $F_{X_1}(x_1)$ for three values of $F_Y(y)$; and (f) scatter plot among the Grade of x_3 and Grade of y.

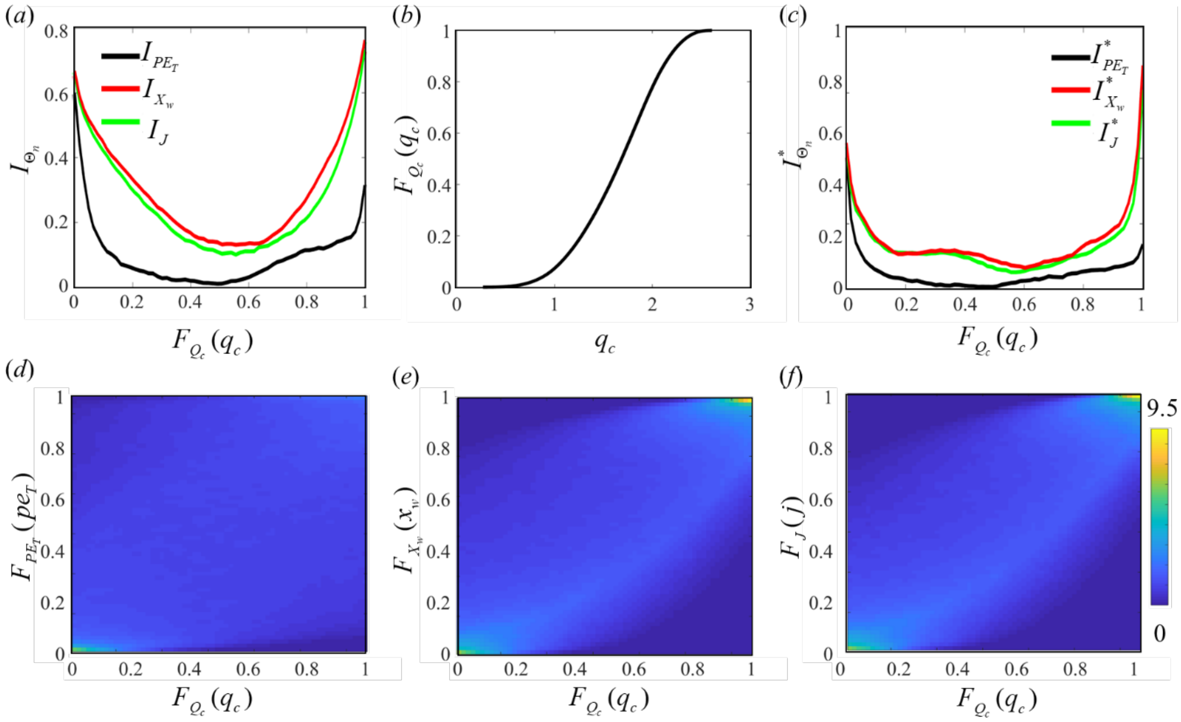

Fig. 2. Results of the copula-density GSA for the critical pumping rate, i.e., Q_c, on the basis of model (8): (*a*) I_{Θ_n} and (*c*) $I^*_{\Theta_n}$ for Θ_n = PE_T, X_w, or *J* against $F_{Q_c}(q_c)$; (*b*) $F_{Q_c}(q_c)$ versus q_c; copula-density between $F_{Q_c}(q_c)$ and (*d*) $F_{PE_T}(pe_T)$, (*e*) $F_{X_w}(x_w)$, or (*f*) $F_J(j)$.

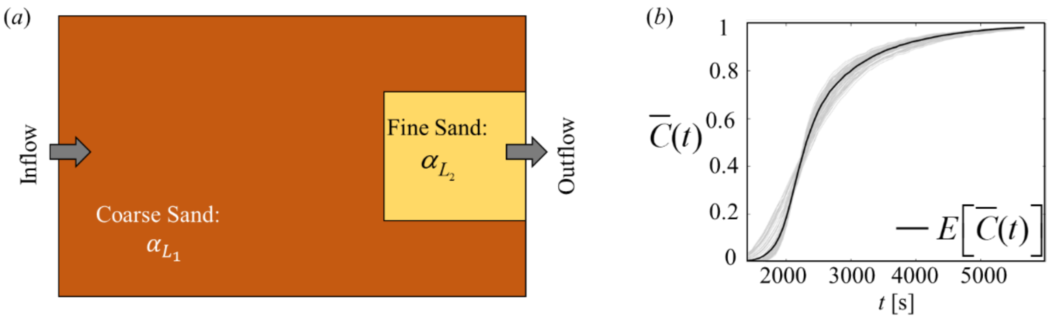

Fig. 3. (*a*) Sketch of the laboratory experimental set-up; (*b*) expected value of the solute concentration at the outlet, i.e., $E\left[\overline{C}(t)\right]$ (black curve), and a sub set of 100 Monte Carlo realizations (grey curves) versus time, t.

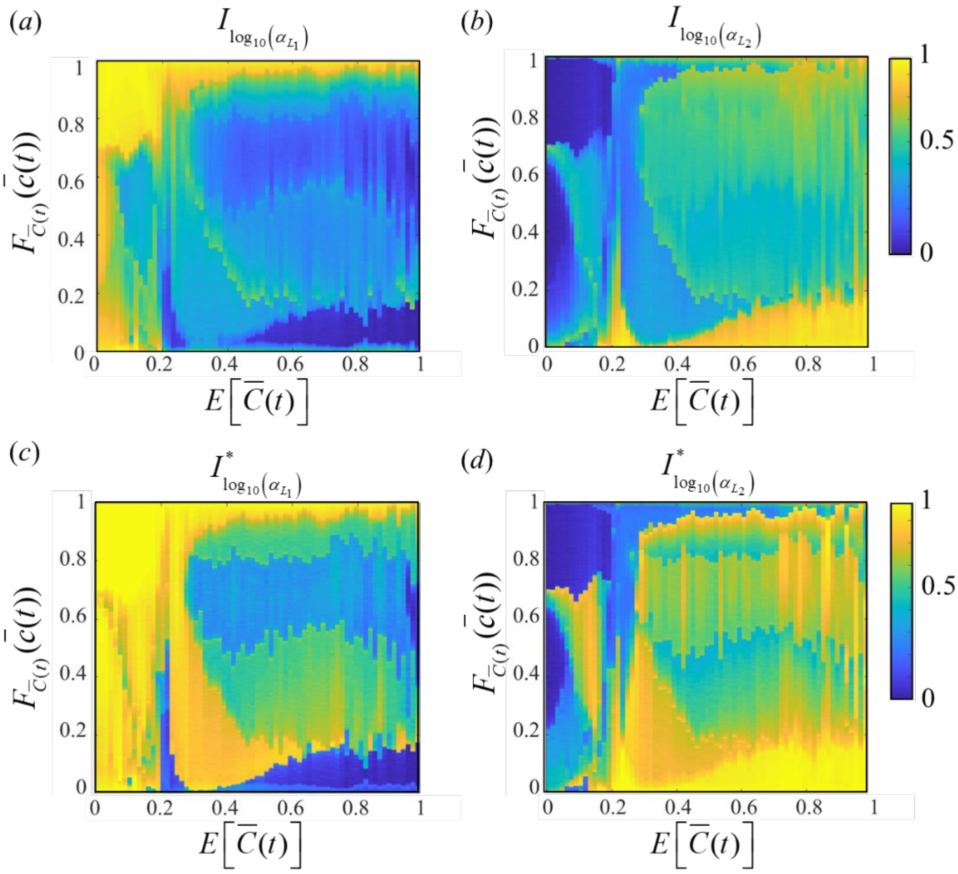

Fig. 4. Results of the copula-density GSA for the solute breakthrough curve, i.e., $\overline{C}(t)$: (a) $I_{\log_{10}(\alpha_{L_1})}$, ($b$) $I_{\log_{10}(\alpha_{L_2})}$, ($c$) $I^*_{\log_{10}(\alpha_{L_1})}$ and (d) $I^*_{\log_{10}(\alpha_{L_2})}$ as a function of $F_{\overline{C}(t)}(\overline{c}(t))$ and of the expected value of $\overline{C}(t)$, i.e., $E\left[\overline{C}(t)\right]$.

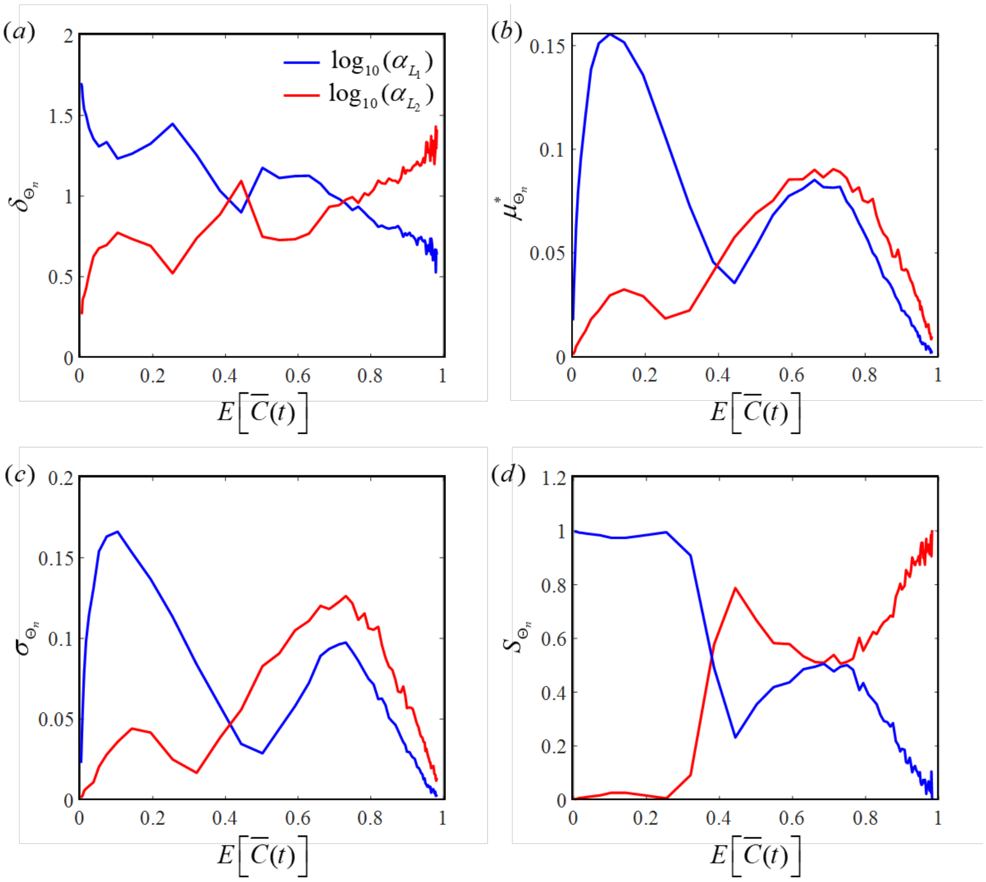

Fig. B1. GSA indices for the solute breakthrough curve, i.e., $\overline{C}(t)$: (*a*) distribution-based index δ_{Θ_n}; Morris' indices (*b*) $\mu^*_{\Theta_n}$ and (*c*) σ_{Θ_n}; principal Sobol' index (*d*) S_{Θ_n} versus the expected value of $\overline{C}(t)$, i.e., $E\left[\overline{C}(t)\right]$. Outcomes for the coarse (blue curves) and fine (red curves) sands are depicted.